Reactions of Electron-Deficient Triosmium Clusters with Diazomethane: Electrochemical Properties and Computational Studies of Charge Distribution

Md. Abdul Mottalib, Noorjahan Begum, S. M. Tareque Abedin, Tahmina Akter, Shariff E. Kabir,* and Md. Arzu Miah

Department of Chemistry, Jahangirnagar University, Savar, Dhaka-1342, Bangladesh

Dalia Rokhsana and Edward Rosenberg*

Department of Chemistry, University of Montana, Missoula, Montana 59812

G. M. Golzar Hossain

Department of Chemistry, University of Wales Cardiff, P.O. Box 912, Park Place, Cardiff CF1 3TB, U.K.

Kenneth I. Hardcastle

Department of Chemistry, Emory University, Atlanta, Georgia 30322

Received May 12, 2005

The 46-electron quinoline triosmium clusters (μ-H)$Os_3(CO)_9(\mu_3$-η^2-$C_9H_5(R)N)$ (**6**, R = 4-CH_3; **7**, R = H) react with excess CH_2N_2 at 0 to 25 °C to give (μ-H)$_2Os_3(CO)_9(\mu_3$-η^2-$CHC_9H_5(R)N)$ (**10**, R = 4-CH_3; **11**, R = H), formed by insertion and subsequent C−H oxidative addition of a CH_2 moiety into the ring C(8)−Os bond. In contrast, the related 46-electron quinoxaline compound (μ-H)$Os_3(CO)_9(\mu_3$-η^2-$C_8H_5N_2)$ (**8**) reacts with excess CH_2N_2 at 0 to 25 °C to give (μ-H)$_2Os_3(CO)_9(\mu_3$-η^2-$CHC_8H_4(5\text{-}CH_3)N_2)$ (**12**), where two CH_2 groups have inserted into the C(5)−H bond as well as the C(8)−Os bond, and (μ-H)$_2Os_3(CO)_9(\mu_3$-η^2-$CHC_8H_5N_2)$ (**13**), the analogue of **11**. The 5-methylquinoxaline compound (μ-H)$Os_3(CO)_9(\mu_3$-η^2-$C_8H_4(5\text{-}CH_3)N_2)$ (**9**) reacts with diazomethane at 0 to 25 °C to give **12** and $Os_3(CO)_9(\mu_3$-η^2-$C_8H_4(5\text{-}CH_3)N_2)$-($\mu$-$CH_2)(CH_3)$ (**14**), containing an edge-bridging methylene group and a σ-bound methyl group. Thermolysis of **10** and **11** at 98 °C yields (μ-H)$_3Os_3(CO)_8(\mu_3$-η^2-$C(C_9H_5)(R)N)$ (**15**, R = 4-CH_3; **16**, R = H), (μ-H)$Os_3(CO)_9(\mu_3$-η^2-$C(C_9H_5)(R)N)$ (**17**, R = 4-CH_3; **18**, R = H), and (μ-H)Os_4-$(CO)_{11}(\mu_3$-η^2-$C(C_9H_5)(R)N)$ (**19**, R = 4-CH_3; **20**, R = H). The trihydrides **15** and **16** are formed by a further C−H activation of the coordinated methylidene group of **10** and **11**, respectively. Thermolysis of **10** and **11** in the presence of H_2 at 1 atm at 80 °C gives **15** and **16** in high yields. The solid-state structure of **17** reveals that the methylidyne carbon atom has a significant bonding interaction with the osmium atom coordinated to nitrogen. Thermolysis of **12** and **13** at 98 °C gives (μ-H)$Os_3(CO)_9(\mu_3$-η^2-$CC_8H_4(R)N_2)$ (**21**, R = 5-CH_3; **22**, R = H), whereas a similar thermolysis in the presence of H_2 (1 atm) at 80 °C gives (μ-H)$_3Os_3(CO)_8$-$(\mu_3$-η^2-$CC_8H_4(5\text{-}CH_3)N_2)$ (**23**, R = 5-CH_3; **24**, R = H). The compounds **12**, **13**, **23**, and **24** all show one-electron reversible reductions, and the reduction potentials are similar to previously studied quinoxaline clusters. DFT calculations show that most of the spin density is confined to the heterocyclic ligand, and this explains the similarity between the observed reduction potentials for the products with different bonding modes to cluster but containing the same heterocycle. The qualitative correlation between the calculated natural charges and the distribution of unpaired spin densities in **12** and **13** corroborate this conclusion. The molecular structures of **10**, **12**, **13**, **17**, and **20** have been determined by single-crystal X-ray diffraction studies.

Introduction

Organic diazo compounds are highly reactive substrates having several reaction centers in one molecule.[1,2] This makes them promising reagents for the synthesis of functionalized organometallic complexes. Reactions of diazoalkanes with transition metal complexes often result in the formation of carbene complexes with concurrent liberation of N_2.[3,4] This is a key reaction in catalytic processes such as carbene insertion into C−H bonds, cyclopropanation of olefins, Fischer−Trop-

(1) Lemenovskii, D. A.; Putala, M.; Nikonov, G. I.; Kazennova, N. B.; Yufit, D. S.; Struchkov, Yu. T. *J. Organoment. Chem*. **1993**, *454*, 123, and references therein.

(2) Mizobe, Y.; Ishii, Y.; Hidai, M. *Coord. Chem. Rev*. **1995**, *139*, 281, and references therein.

10.1021/om0503794 CCC: $30.25
Publication on Web 08/17/2005

sch synthesis, and alkyne isomerization.[5] The reactions of diazoalkanes with both coordinatively unsaturated and saturated trimetallic complexes of osmium, ruthenium, and iron have been investigated by several groups and have been found to give many interesting compounds with various coordination modes.[6−21] For example, the saturated triosmium acetonitrile compound $Os_3(CO)_{11}(MeCN)$ reacts with CH_2N_2 to yield $Os_3(\mu\text{-}CO)(CO)_{10}(\mu\text{-}CH_2)$,[6,7] whereas the coordinatively unsaturated cluster $(\mu\text{-}H)_2Os_3(CO)_{10}$ gives $(\mu\text{-}H)_2Os_3(CO)_{10}(\mu\text{-}CH_2)$, which exists in equilibrium with $(\mu\text{-}H)Os_3(CO)_{10}(\mu\text{-}CH_3)$.[8] The parent iron compound, $Fe_3(CO)_{12}$, reacts with diphenyldiazomethane to give $Fe_3(CO)_9(NNCPh_2)_2$, containing the $\mu_3\text{-}\eta^1$-diazoalkane ligand.[9] On the contrary, the ruthenium analogue, $Ru_3(CO)_{12}$, reacts with diazomethane to give $Ru_3(\mu\text{-}CO)(CO)_{10}(\mu\text{-}CH_2)$, which rearranges to the hydrido ketenylidene compound $(\mu\text{-}H)_2Ru_3(CO)_9(\mu\text{-}CCO)$ at 45 °C. The latter reacts further with CH_2N_2 to give the C−C coupling product, $(\mu\text{-}H)_2Ru_3(CO)_9(CCH_2)$.[10] The dppm-substituted compound, $Ru_3(CO)_{10}(\mu\text{-dppm})$, reacts with CH_2N_2 to afford the μ-methylene compound, $Ru_3(CO)_7(\mu_3\text{-}\eta^3\text{-}C(O)CH_2)(\mu\text{-}CH_2)(\mu\text{-dppm})$, which readily reacts with CO to give the dinuclear complex, $Ru_2(CO)_5(\mu\text{-}\eta^4\text{-}CH_2C(O)CH_2)(\mu\text{-dppm})$.[11] There have been several reports on the coupling of μ_3-imidoyls[19] or μ_3-alkynes[14,18] with μ-methylenes or η^1-carbenes[22] in trinuclear clusters of osmium and ruthenium. For example, the μ_3-imidoyl clusters $(\mu\text{-}H)Os_3(CO)_9(\mu_3\text{-}\eta^2\text{-}C{=}NCH_2CH_2CH_2-)$ react with CH_2N_2 to afford $(\mu\text{-}H)_2Os_3(CO)_9(\mu_3\text{-}\eta^2\text{-}CH\text{-}C{=}NCH_2CH_2CH_2-)$, in which a methylene fragment has inserted into the carbon−metal σ-bond of the imidoyl ligand and underwent a C−H oxidative addition.[19]

Scheme 1

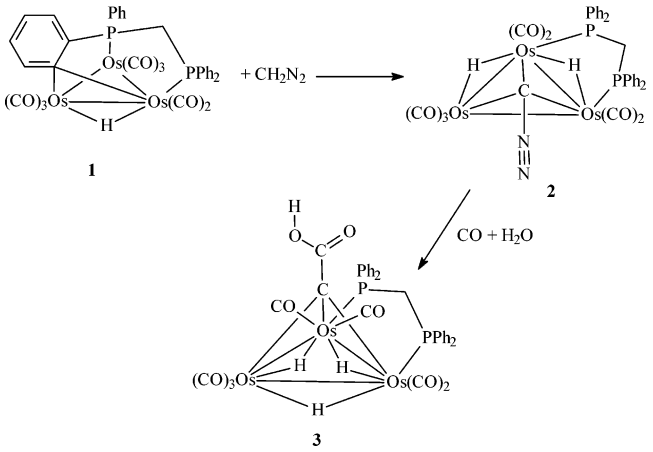

We have been investigating the reactivity of a novel class of electron-deficient complexes of the general formula $(\mu\text{-}H)Os_3(CO)_9(\mu_3\text{-}\eta^2\text{-L-H})$ (L = benzoheterocycle) where the electron deficiency arises from the presence of a three-center two-electron bond β to the coordinated pyridinyl nitrogen.[23] The reactions of these complexes with neutral nucleophiles such as phosphines and amines result in ligand addition at the metal core,[23a,b] while with anionic nucleophiles such as hydride or carbanions nucleophilic addition is at the carbocyclic ring.[23c,24] Most recently, we have demonstrated that despite their structural similarities, the reactivity of these complexes is sensitive to the nature of the heterocyclic ring.[24,25]

In a preliminary communication we reported[20] that the coordinately unsaturated compound $(\mu\text{-}H)Os_3(CO)_8(Ph_2PCH_2P(Ph)C_6H_4)$ (**1**) reacts with CH_2N_2 to give the novel compound $(\mu\text{-}H)_2Os_3(CO)_7(\mu_3\text{-}CN_2)(\mu\text{-dppm})$ (**2**), which reacts with CO and H_2O to give $(\mu\text{-}H)_3Os_3(CO)_7(\mu_3\text{-CCOOH})(\mu\text{-dppm})$ (**3**) (Scheme 1). We have also reported[21] that in the case of the unsaturated cluster $(\mu\text{-}H)Os_3(CO)_9(\mu_3\text{-}\eta^2\text{-}C_7H_3(2\text{-}CH_3)NS)$ (**4**) the reaction with diazomethane proceeds in a completely different way to give $Os_3(CO)_9(\mu\text{-}\eta^2\text{-}C_7H_3(2\text{-}CH_3)NS)(\mu\text{-}CH_2)CH_3$ (**5**), containing an edge-bridging methylene group and

(3) (a) Herrmann, W. A. *Angew. Chem., Int. Ed. Engl.* **1978**, *17*, 800. (b) Herrmann, W. A. *Adv. Organomet. Chem.* **1982**, *20*, 159.
(4) (a) Feldman, J.; Schrock, R. R. *Prog. Inorg. Chem.* **1991**, *39*, 1. (b) Gallop, M. A.; Roper, W. R. *Adv. Organomet. Chem.* **1986**, *25*, 121.
(5) Gambarotta, S.; Bert, M. B.; Floriani, C.; Guastrini, A. *J. Chem. Soc., Chem. Commun.* **1982**, 374.
(6) Shapley, J. R.; Sievert, A. C.; Churchill, M. R.; Wasserman, H. J. *J. Am. Chem. Soc.* **1981**, *103*, 6975.
(7) Johnson, B. F. G.; Lewis, J.; Raithby, P. R.; Sankey, S. W. *J. Organomet. Chem.* **1982**, *231*, C65.
(8) (a) Calvert, R. B.; Shapley, J. R. *J. Am. Chem. Soc.* **1977**, *99*, 5225. (b) Calvert, R. B.; Shapley, J. R. *J. Am. Chem. Soc.* **1978**, *100*, 7726. (c) Calvert, R. B.; Shapley, J. R.; Schultz, A. J.; Williams, J. M.; Suib, S. L.; Stucky, G. D. *J. Am. Chem. Soc.* **1978**, *100*, 6240. (d) Shultz, A. J.; Williams, J. M.; Calvert, R. B.; Shapley, J. R.; Stucky, G. D. *Inorg. Chem.* **1979**, *18*, 319.
(9) Baikie, P. E.; Mills, O. S. *J. Chem. Soc., Chem. Commun.* **1967**, 1228.
(10) Holmgren, J. S.; Shapley, J. R. *Organometallics* **1985**, *4*, 793.
(11) Holmgren, J. S.; Shapley, J. R.; Wilson, S. R.; Pennington, W. T. *J. Am. Chem. Soc.* **1986**, *108*, 508.
(12) Keijsper, J.; Polm, L. H.; Koten, G. van; Vrieze, K.; Goubitz, K.; Stam, C. H. *Organometallics* **1985**, *4*, 1876.
(13) Nucciarone D.; MacLaughlin, S. A.; Taylor, N. J.; Carty, A. J. *Organometallics* **1988**, *7*, 106.
(14) Nucciarone, D.; Taylor, N. J.; Carty, A. J. *Organometallics* **1984**, *3*, 177.
(15) Johnson, B. F. G.; Lewis, J.; Raithby, P. R.; Sankey, S. W. *J. Organomet. Chem.* **1982**, *231*, C65.
(16) Farrugia, L. J.; Green, M.; Hankey, D. R.; Murray, M.; Orpen, A. G.; Stone, F. G. A. *J. Chem. Soc., Dalton Trans.* **1985**, 177.
(17) Green, M.; Hankey, D. R.; Murry, M.; Orpen, A. G.; Stone, F. G. A. *J. Chem. Soc., Chem. Commun.* **1981**, 689.
(18) Clauss, A. D.; Shapley, J. R.; Wilson, J. R. *J. Am. Chem. Soc.* **1981**, *103*, 7387.
(19) Day, M.; Freeman, W.; Hardcastle, K. I.; Tsomaki, M.; Kabir, S. E.; McPhillips, T.; Rosenberg, E.; Scott, L. G.; Wolf, E. *Organometallics* **1992**, *11*, 3376.
(20) Abedin, S. M. T.; Hardcastle, K. I.; Kabir, S. E.; Malik, K. M. A.; Mottalib, Md. A.; Rosenberg, E.; Abedin, Md. J. *Organometallics* **2000**, *19*, 5623.
(21) Kabir, S. E.; Malik, K. M. A.; Mandal, H. S.; Mottalib, Md. A.; Abedin, Md. J.; Rosenberg, E. *Organometallics* **2002**, *21*, 2593.
(22) Beans, L. R.; Keister, J. B. *Organometallics* **1985**, *4*, 1713.
(23) (a) Kabir, S. E.; Kolwaite, D. S.; Rosenberg, E.; Hardcastle, K. I.; Cresswell, W.; Grindstaff, J. *Organometallics* **1995**, *14*, 3611. (b) Arcia, E.; Rosenberg, E.; Kolwaite, D. S.; Hardcastle, K. I.; Ciurash, J.; Duque, R.; Gobetto, R.; Milone, L.; Osella, D.; Botta, M.; Dastru', W.; Viale, A.; Fiedler, J. *Organometallics* **1998**, *17*, 415. (c) Rosenberg, E.; Spada, F.; Sugden, K.; Martin, B.; Milone, L.; Gobetto, R.; Viale, A.; Fiedler, J. *J. Organomet. Chem.* **2003**, *668*, 51. (d) Abedin, M. J.; Bergman, B.; Holmquist, R.; Smith, R.; Rosenberg, E.; Ciurash, J.; Hardcastle, K. I.; Roe, J.; Vazquez, V.; Roe, C.; Kabir, S. E.; Roy, B.; Alam, S.; Azam, K. A. *Coord. Chem. Rev.* **1999**, *190−192*, 175. (e) Bergman, B.; Holmquist, R.; Smith, R.; Rosenberg, E.; Hardcastle, K. I.; Visi, M.; Ciurash, J. *J. Am. Chem. Soc.* **1998**, *120*, 12818. (f) Smith, R.; Rosenberg, E.; Hardcastle, K. I.; Vazquez, V.; Roh, J. *Organometallics* **1999**, *18*, 3519. (g) Bar Din, A. V.; Bergman, B.; Rosenberg, E.; Smith, R.; Dastru', W.; Gobetto, R.; Milone, L.; Viale, A. *Polyhedron* **1998**, *17*, 2975. (h) Rosenberg, E.; Abedin, Md. J.; Rokhsana, D.; Osella, D.; Milone, L.; Nervi, N.; Fiedler, J. *Inorg. Chim. Acta* **2000**, *300−302*, 769.
(24) Rosenberg, E.; Kabir, S. E.; Abedin, Md. J.; Hardcastle, K. I. *Organometallics* **2004**, *23*, 3982.
(25) (a) Nervi, C.; Gobetto, R.; Milone, L.; Viale, A.; Rosenberg, E.; Rokhsana, D.; Fiedler, J. *Chem. Eur. J.* **2003**, *9*, 5749. (b) Rosenberg, E.; Rokhsana, D.; Nervi, C.; Gobetto, R.; Milone, L.; Viale, A.; Fiedler, J.; Botavina, M. A. *Organometallics* **2004**, *23*, 215. (c) Rosenberg, E.; Abedin, M. J.; Rokhsana, D.; Viale, A.; Dastru', W.; Gobetto, R.; Milone, L.; Hardcastle, K. I. *Inorg. Chim. Acta* **2002**, *334*, 343.

Scheme 2

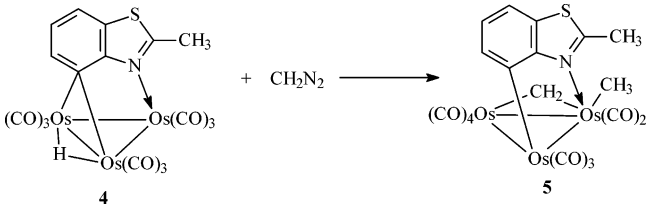

4 **5**

Scheme 3

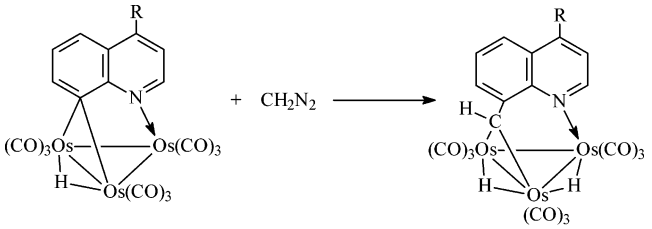

6, R=CH_3
7, R=H

10, R=CH_3
11, R=H

a σ-bound methyl group[21] (Scheme 2). The above observations suggested remarkable sensitivity of the regiochemistry of methylene addition toward the structure of the heterocycle and prompted us to examine the reactivity of the related 46-electron triosmium compounds (μ-H)$Os_3(CO)_9(\mu_3$-η^2-C_9H_5(R)N) (**6**, R = 4-CH_3; **7**, R = H) and (μ-H)$Os_3(CO)_9(\mu_3$-η^2-C_8H_4(R)N_2) (**8**, R = H; **9**, R = 5-CH_3) with diazomethane. We were particularly interested to see how the reactivity of these aza and diaza heterocycles with diazomethane compared with the previously reported thioaza heterocycles. We report here an examination of these reactions as well as an investigation of the electrochemical properties of the products in an attempt to gain a further understanding of how changes in the bonding mode of a complex organic molecule to a trimetallic core impacts its electron acceptor properties and the stability of the resulting radical anion. For the radical anions that were found to be stable on the cyclic voltammetry (CV) time scale we have performed ab initio density functional theory (DFT) calculations in order to elucidate the electron distribution in these systems.

Results and Discussion

In sharp contrast to the reaction of the 2-methylbenzothiazole triosmium compound **4** with CH_2N_2, which afforded the μ-methylidene σ-methyl compound **5**,[21] the reactions of the electron-deficient clusters **6** and **7** with excess CH_2N_2 at 0 to 25 °C give (μ-H)$_2Os_3(CO)_9(\mu_3$-η^2-CHC_9H_5(R)N) (**10**, R = 4-CH_3; **11**, R = H) in 80 and 85% yields, respectively (Scheme 3).

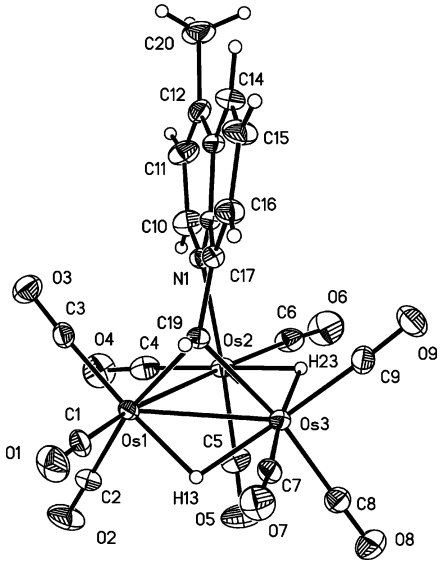

Figure 1. Molecular geometry of (μ-H)$_2Os_3(CO)_9(\mu_3$-η^2-CHC_9H_5(4-CH_3)N), **10**, showing the calculated position of the hydrides. Thermal ellipsoids are drawn at the 50% probability level.

These compounds are presumably formed by insertion of the methylene group into the metal−carbon σ-bond of the quinoline ligands followed by C−H oxidative addition. In contrast, addition of excess ethereal diazomethane to a dichloromethane solution of the quinoxaline unsaturated compound **8** at 0 to 25 °C affords two new compounds, (μ-H)$_2Os_3(CO)_9(\mu_3$-η^2-CHC_8H_4-(5-CH_3)N_2) (**12**) and (μ-H)$_2Os_3(CO)_9(\mu_3$-η^2-$CHC_8H_5N_2$) (**13**), in 20 and 35% yields, respectively (Scheme 4). All the compounds have been characterized by spectroscopic data together with single-crystal X-ray diffraction analyses for **10**, **12**, and **13**.

The solid-state structures of **10** and **12** are shown in Figures 1 and 2, respectively, crystal data are given in Table 1, and selected bond distances and angles are summarized in Tables 2 and 3, respectively. The basic cores of both the molecules are the same, having a triangular metal framework of osmium atoms with three distinctly different osmium−osmium bond lengths (Os(1)−Os(2) = 2.7919(4), Os(2)−Os(3) = 2.9913(4), and Os(1)−Os(3) = 2.8323(4) Å for **10** and Os(1)−Os(2) = 2.9959(7), Os(2)−Os(3) = 2.8070(7), and Os(1)−Os(3) = 2.8283(7) Å for **12**) and nine terminal carbonyl ligands, three on each metal atom. The hydride ligands for both **10** and **12** were located using the program WinGX.[26] In case of **10**, the hydride ligand H(23) is located at the elongated Os(2)−Os(3) edge, which is also bridged by the heterocyclic ligand, μ_3-η^2-CHC_9H_5(4-CH_3)N, while the other hydride H(13) shares the same shortest

Scheme 4

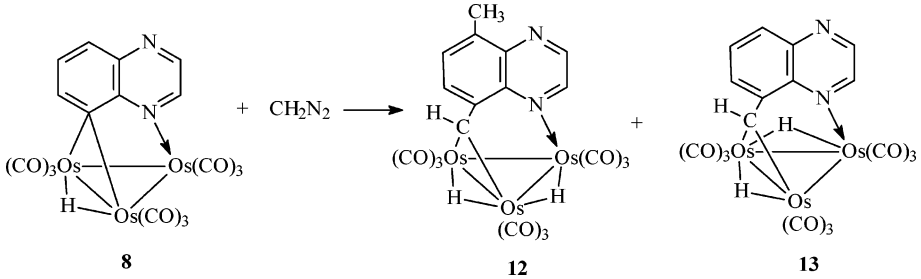

8 **12** **13**

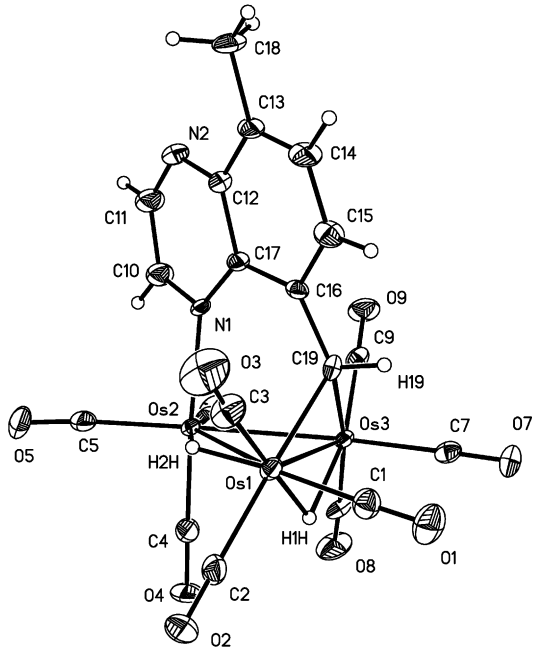

Figure 2. Molecular geometry of (μ-H)$_2$Os$_3$(CO)$_9$(μ_3-η^2-CHC$_8$H$_4$(5-CH$_3$)N$_2$), **12**, showing the calculated position of the hydrides. Thermal ellipsoids are drawn at the 50% probability level.

Os(1)−Os(2) edge as the alkylidene carbon and is well-tucked well below the Os$_3$ triangle. Similarly, for **12**, the hydrides are found to bridge the Os(1)−Os(2) and Os(1)−Os(3) edges of the Os triangle in which the Os(1)−Os(2) edge is bridged by the N atom of the heterocyclic ligand, μ_3-η^2-CHC$_8$H$_4$(5-CH$_3$)N$_2$, while the Os(1)−Os(3) edge is bridged by the methylidene carbon of the ligand. These observations are analogous to that reported for (μ-H)$_2$Os$_3$(CO)$_9$(μ_3-η^2-CHC=NCH$_2$CH$_2$CH$_2$−), in which metal−metal bonds bridged by heterocyclic and hydride ligands are significantly longer than the other bridging metal−metal bonds.[19] The bridging positions of the hydrides in **10** are further supported by the orientation of carbonyl groups CO(3), CO(9), CO(4), and CO(7), which were essentially *trans* to the metal hydrogen bond vectors, maintaining approximately octahedral geometry. The μ-alkylidene carbon bridges Os(1) and Os(3) almost symmetrically (Os(1)−C(19) = 2.159(4), Os(3)−C(19) = 2.151(4) Å for **10** and Os(1)−C(19) = 2.158(5), Os(3)−C(19) = 2.151(5) Å), and the nitrogen is coordinated to Os(2) with Os(2)−N(1) bond lengths of 2.203(4) Å for **10** and 2.191(4) Å for **12**, which are significantly longer than the corresponding bond length in **6** (2.13(2) Å)[23a] but is comparable to the Os−N bond length in (μ-H)Os$_3$(CO)$_{10}$(μ-1,8-η^2-C$_9$H$_6$N).[27] An intriguing feature of **12** is the presence of the 5-methyl group on the quinoxaline ring that most probably has been formed by insertion of a second methylene group into the C(5)−H bond of the quinoxaline ligand. Both clusters **10** and **12** contain 48 valence electrons, as expected for an electron-precise trinuclear cluster containing three metal−metal bonds, and each metal atom achieves an 18-electron configuration. The spectroscopic data for **10** and **12** are in accord with the solid-state structure, and the spectroscopic data for **11** indicate that it is a direct analogue of **10** and **12**.

The solid-state structure of **13** is shown in Figure 3, crystal data are given in Table 1, and selected bond distances and angles are collected in Table 4. Compound **13** crystallizes in the triclinic space group with two crystallographically independent and enantiomeric molecules in the unit cell. Each molecule consists of an Os$_3$ triangle with three different metal−metal bonds and nine terminal carbonyl ligands, three bonded to each osmium atom. The molecules differ in the relative location of the cluster-bound hydride ligands. In molecule 1 (Figure 3), one of the hydrides bridges the unbridged Os(3)−Os(2) edge, which is supported by the observation that this edge is significantly elongated (3.0059(7) Å) compared to the methylidyne carbon-bridged Os(3)−Os(1) edge (2.8365(7) Å). This edge is also spanned by the other hydride ligand. The heterocyclic ligand bridges the Os(2)−Os(1) edge (2.7986(7) Å). However, in molecule 2, one of the hydrides bridges the Os(2)−Os(1) edge, which is simultaneously bridged by the heterocyclic ligand and is also consistent with substantially elongated bond (2.9981(7) Å) compared to the other two Os−Os distances (Os(3)−Os(1) = 2.8365(7), Os(2)−Os(3) = 2.8013(7) Å). As in molecule 1, the remaining hydride bridges the Os(3)−Os(1) edge, which is simultaneously bridged by the methylidene carbon atom, and the Os(3)−Os(1) distances in the two molecules are exactly the same (2.8365(7) Å in molecule 1 and 2.8365(7) Å in molecule 2). The dimensions of heterocyclic ligands in the two molecules are similar. Thus C(16)−N(2), C(17)−N(1), C(13)−C(14), and C(11)−C(12) bond distances in molecule 1 are 1.32(2), 1.357(17), 1.34(2), and 1.401(18) Å, respectively, while the corresponding distances in molecule 2 are 1.30(3), 1.321(2), 1.31(3), and 1.360(18) Å, respectively. The spectroscopic data of **13** are consistent with the solid-state structures.

The unusual formation of **12** from the above reaction was further substantiated by synthesizing the 5-methyl quinoxaline electron-deficient compound (μ-H)Os$_3$(CO)$_9$(μ_3-η^2-C$_8$H$_4$(5-CH$_3$)N (**9**) followed by reaction with CH$_2$N$_2$. The reaction of **9** with excess diazomethane gives **12** and Os$_3$(CO)$_9$(μ_3-η^2-C$_8$H$_4$(5-CH$_3$)N$_2$)(μ-CH$_2$)(CH$_3$) (**14**) (Scheme 5) in 49 and 11% yields, respectively. Compound **14** has been characterized by elemental analysis and infrared and ^{1}H NMR spectroscopic data. The formation of **14** can be viewed as resulting from the insertion of a methylene group into one of the metal−metal bonds followed by the interaction of the second methylene with the cluster-bound bridging hydride. The reverse sequence, formation of a methyl group followed by reaction with a second methylene, is also possible. To our knowledge compound **14** provides the second example of a triosmium cluster containing both bridging methylene and σ-bonded methyl groups, the first being **5**.[21]

Thermolysis of **10** and **11** at 98 °C affords two trinuclear compounds, (μ-H)$_3$Os$_3$(CO)$_8$(μ_3-η^2-C(C$_9$H$_5$)(R)N) (**15**, R = 4-CH$_3$, 17%; **16**, R = H, 15%) and (μ-H)Os$_3$(CO)$_9$(μ_3-η^2-C(C$_9$H$_5$)(R)N) (**17**, R = 4-CH$_3$, 30%; **18**, R = H, 36%), and one tetranuclear compound, (μ-H)Os$_4$(CO)$_{11}$(μ_3-η^2-C(C$_9$H$_5$)(R)N) (**19**, R = 4-CH$_3$, 15%; **20**,

(26) Farrugia, L. J. *J. Appl. Crystallogr.* **1999**, *32*, 837.
(27) Akter, J.; Hossain, G. M. G.; Kabir, S. E.; Malik, K. M. A. *J. Chem. Crystallogr.* **2000**, *12*, 773.

Table 1. Crystal Data and Structure Refinement for 10, 12, 13, 17, and 20

	10	**12**	**13**
empirical formula	$C_{20}H_{11}NO_9Os_3$	$C_{19}H_{10}N_2O_9Os_3$	$C_{18}H_8N_2O_9Os_3$
fw	979.90	980.89	966.88
temperature (K)	173(2)	173(2)	150(2)
wavelength Å	0.71073	0.71073	0.71073
cryst syst	triclinic	triclinic	triclinic
space group	$P\bar{1}$	$P\bar{1}$	$P\bar{1}$
unit cell dimens			
a (Å)	9.6788(12)	9.487(2)	11.2089(4)
b (Å)	10.4164(14)	10.269(3)	12.7527(5)
c (Å)	11.5639(15)	11.790(3)	15.4816(7)
α (deg)	100.764(3)	98.686(7)	85.582(2)
β (deg)	90.929(3)	90.684(9)	89.192(2)
γ (deg)	100.978(3)	99.636(7)	84.136(2)
V (Å^3)	1122.8(3)	1118.6(5)	2194.83(15)
Z	2	2	4
density$_{calc}$ (mg/m^3)	2.899	2.912	2.923
abs coeff (cm^{-1})	16.985	17.049	17.376
F(000)	876	876	1710
cryst size (mm)	0.22 × 0.20 × 0.16	0.40 × 0.36 × 0.22	0.25 × 0.22 × 0.18
θ range for data collection (deg)	1.80 to 28.33	1.75 to 28.29	2.16 to 26.38
limiting indices	$-12 \le h \le 12$ $-13 \le k \le 13$ $-15 \le l \le 15$	$-12 \le h \le 12$ $-13 \le k \le 13$ $-15 \le l \le 15$	$-14 \le h \le 14$ $-15 \le k \le 15$ $-19 \le l \le 19$
no. of reflns collected	11 751	15 327	22 944
no. of indep reflns	5571 [R_{int} = 0.025]	5533 [R_{int} = 0.0418]	8855 [R_{int} = 0.1045]
refinement method	full-matrix least-squares on F^2	full-matrix least-squares on F^2	full-matrix least-squares on F^2
no. of data/restraints/params	5571/0/299	5533/0/299	8855/0/577
goodness-of-fit on F^2	1.035	1.024	1.014
final R indices [$I > 2\sigma(I)$]	R_1 = 0.0243, wR_2 = 0.0578	R_1= 0.0265, wR_2 = 0.0674	R_1 = 0.0566, wR_2 = 0.1362
R indices (all data)	R_1 = 0.0270, wR_2 = 0.0589	R_1= 0.0292, wR_2 = 0.0688	R_1= 0.0750, wR_2 = 0.1479
largest diff peak and hole (e Å^{-3})	1.693 and −2.272	1.637 and −2.324	3.362 and −3.901

	17	**20**
empirical formula	$C_{20}H_9NO_9Os_3$	$C_{21}H_7NO_{11}Os_4$
fw	977.90	1210.07
temperature (K)	150(2)	293(2)
wavelength Å	0.71069	0.71073
cryst syst	monoclinic	monoclinic
space group	$P2_1/n$	$P2_1/c$
unit cell dimens		
a (Å)	15.731(4)	12.4821(2)
b (Å)	8.900(2)	12.4363(2)
c (Å)	16.263(3)	16.2496(2)
α (deg)		
β (deg)	100.16(2)	104.0791(8)
γ (deg)		
volume (Å^3)	2241.2(9)	2446.67(6)
Z	4	4
density$_{calc}$ (mg/m^3)	2.901	3.282
abs coefficient (cm^{-1})	17.017	20.767
F(000)	1748	2124
cryst size (mm)	0.25 × 0.22 × 0.15	0.22 × 0.15 × 0.12
θ range for data collection (deg)	1.98 to 25.06	1.68 to 27.51
limiting indices	$-10 \le h \le 17$ $-8 \le k \le 10$ $-18 \le l \le 18$	$-16 \le h \le 16$ $-16 \le k \le 16$ $-21 \le l \le 21$
no. of reflns collected	8001	54 059
no. of indep reflns	3355 [R_{int} = 0.0684]	5626 [R_{int} = 0.0914]
refinement method	full-matrix least-squares on F^2	full-matrix least-squares on F^2
no. of data/restraints/params	3355/48/299	5626/0/334
goodness-of-fit on F^2	0.962	1.116
final R indices [$I > 2\sigma(I)$]	R_1 = 0.0332, wR_2 = 0.0845	R_1 = 0.0312, wR_2 = 0.0729
R indices (all data)	R_1 = 0.0446, wR_2 = 0.0863	R_1 = 0.0462, wR_2 = 0.082
largest diff peak and hole (e Å^{-}3)	1.542 and −1.620	1.584 and −3.644

R = H, 18%), in addition to a trace amount of the parent compounds **6** and **7**, respectively (Scheme 6).

The structural assignments of **15** and **16** have been made on the basis of spectroscopic analysis (IR, NMR, and mass) and by comparing the spectroscopic data with those reported for (μ-H)$_3$Os$_3$(CO)$_8$(μ_3-η^2-CC$_7$H$_3$(Me)NS), whose structure has been determined by single-crystal X-ray diffraction study.[21] The carbonyl stretching frequencies of **15** and **16** are very similar to those of (μ-H)$_3$Os$_3$(CO)$_8$(μ_3-η^2-CHC$_7$H$_3$(Me)NS), indicating that they have similar structures.[21] The aromatic region of the ^{1}H NMR spectrum of **15** shows three doublets at δ

Table 2. Selected Bond Distances (Å) and Angles (deg) for 10

Bond Distances			
Os(1)−Os(2)	2.7919(4)	C(11)−C(12)	1.362(8)
Os(2)−Os(3)	2.9913(4)	C(12)−C(13)	1.442(7)
Os(1)−Os(3)	2.8323(4)	C(12)−C(20)	1.515(7)
Os(3)−C(19)	2.151(4)	C(13)−C(14)	1.418(7)
Os(1)−C(19)	2.159(4)	C(13)−C(18)	1.428(6)
C(14)−C(15)	1.354(7)	C(18)−N(1)	1.397(6)
C(15)−C(16)	1.393(7)	Os(2)−N(1)	2.203(4)
C(16)−C(17)	1.392(6)	C(10)−C(11)	1.397(7)
C(17)−C(18)	1.438(6)	C(10)−N(1)	1.337(6)
C(17)−C(19)	1.495(6)	C(10)−C(11)	1.397(7)

Bond Angles			
Os(2)−Os(1)−Os(3)	64.258(8)	C(19)−Os(1)−Os(3)	48.80(11)
Os(1)−Os(2)−Os(3)	58.526(11)	C(19)−Os(3)−Os(1)	49.03(12)
Os(1)−Os(3)−Os(2)	57.216(7)	N(1)−Os(2)−Os(1)	88.72(10)
C(19)−Os(1)−Os(2)	81.06(12)	Os(1)−C(19)−Os(3)	82.17(15)
Os(3)−Os(2)−C(6)	115.38(16)	Os(3)−Os(1)−C(2)	119.61(15)
Os(2)−Os(3)−C(9)	110.18(14)	Os(1)−Os(3)−C(7)	95.39(14)

Table 3. Selected Bond Distances (Å) and Angles (deg) for 12

Bond Distances			
Os(1)−Os(2)	2.9959(7)	C(12)−C(17)	1.449(7)
Os(2)−Os(3)	2.8070(7)	C(13)−C(14)	1.359(8)
Os(1)−Os(3)	2.8283(7)	C(13)−C(18)	1.515(7)
Os(1)−C(19)	2.158(5)	C(14)−C(15)	1.401(7)
Os(3)−C(19)	2.151(5)	C(15)−C(16)	1.401(7)
Os(2)−N(1)	2.191(4)	C(16)−C(17)	1.438(7)
C(10)−C(11)	1.392(8)	C(16)−C(19)	1.489(6)
C(11)−N(2)	1.291(8)	C(17)−N(1)	1.394(6)
C(12)−N(2)	1.359(7)	C(12)−C(13)	1.425(7)
C(10)−N(1)	1.331(7)		

Bond Angles			
Os(3)−Os(2)−Os(1)	58.230(18)	C(1)−Os(1)−Os(3)	94.41(17)
Os(2)−Os(3)−Os(1)	64.229(12)	C(8)−Os(3)−Os(1)	120.10(17)
Os(3)−Os(1)−Os(2)	57.541(12)	C(3)−Os(1)−Os(2)	111.23(19)
C(5)−Os(2)−Os(1)	114.02(19)	C(19)−Os(3)−Os(1)	49.09(13)
N(1)−Os(2)−Os(3)	89.56(11)	C(19)−Os(1)−Os(3)	44.88(13)
		Os(3)−C(19)−Os(1)	82.03(17)

8.96, 7.82, and 7.08, a triplet at δ 7.52, and a doublet of doublets at δ 7.25, each integrating for one hydrogen atom, while **16** gives two doublets of doublets at δ 7.12 and 8.14, a multiplet at δ 7.48, a triplet at δ 7.30, and a doublet at δ 9.12 in a relative intensity of 1:1:2:1:1. The high-field triplets at δ −17.11, −18.08, and −18.81

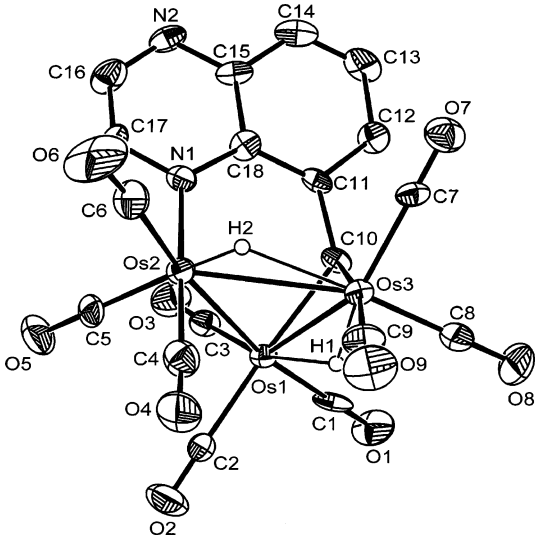

Figure 3. ORTEP drawing of (μ-H)$_2$Os$_3$(CO)$_9$(μ_3-η^2-CHC$_8$H$_5$N$_2$), **13** (molecule A). Thermal ellipsoids are drawn at the 35% probability level.

Table 4. Selected Bond Distances (Å) and Angles (deg) for 13

Bond Distances	molecule 1	molecule 2
Os(1)−Os(2)	2.7986(7)	2.9981(7)
Os(2)−Os(3)	3.0059(7)	2.8013(7)
Os(1)−Os(3)	2.8366(7)	2.8365(7)
Os(2)−N(1)	2.189(11)	2.214(10)
Os(1)−C(10)	2.146(12)	2.176(12)
Os(3)−C(10)	2.179(11)	2.152(12)
N(1)−C(17)	1.357(17)	1.321(17)
N(2)−C(16)	1.32(2)	1.30(3)
N(1)−C(18)	1.390(17)	1.392(16)
N(2)−C(15)	1.352(17)	1.33(2)
C(10)−C(11)	1.498(17)	1.502(16)
C(11)−C(18)	1.422(19)	1.421(18)
C(13)−C(14)	1.34(2)	1.31(3)
C(15)−C(18)	1.456(18)	1.444(17)
C(11)−C(12)	1.404(18)	1.360(18)
C(12)−C(13)	1.41(2)	1.39(2)
C(14)−C(15)	1.42(2)	1.42(3)
C(16)−C(17)	1.34(2)	1.38(2)

Bond Angles	molecule 1	molecule 2
Os(1)−Os(2)−Os(3)	58.378(17)	58.446(17)
Os(2)−Os(1)−Os(3)	64.468(18)	57.306(17)
Os(1)−Os(3)−Os(2)	57.153(17)	64.248(18)
C(3)−Os(1)−Os(2)	93.6(5)	108.9(4)
C(2)−Os(1)−Os(2)	92.5(4)	96.3(5)
C(2)−Os(1)−Os(3)	120.3(4)	122.0(5)
N(1)−Os(2)−Os(1)	88.3(3)	97.5(3)
Os(1)−C(10)−Os(3)	82.0(4)	81.9(4)
C(1)−Os(1)−Os(2)	168.3(5)	154.1(4)
C(10)−Os(1)−Os(2)	82.6(3)	77.6(3)
C(1)−Os(1)−Os(3)	103.9(5)	97.0(4)
C(10)−Os(1)−Os(3)	49.5(3)	48.7(3)
C(5)−Os(2)−N(1)	88.8(5)	90.4(5)
C(6)−Os(2)−Os(1)	172.9(5)	144.4(5)
C(10)−Os(3)−Os(1)	48.5(3)	49.3(3)
C(10)−Os(3)−Os(2)	77.2(4)	82.6(3)

Scheme 5

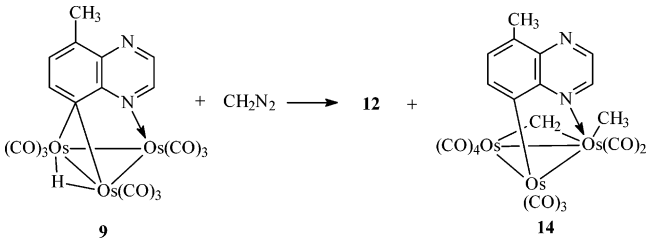

(J = 2.2 Hz) for **15** and δ −16.98, −18.10, and −18.65 (J = 2.0 Hz) for **16**, each integrating for one hydrogen atom, are consistent with the presence of three nonequivalent bridging hydride ligands. All the spectroscopic features of **15** and **16** are very similar to those of (μ-H)$_3$Os$_3$(CO)$_8$(μ_3-η^2-CHC$_7$H$_3$(Me)NS).[21] The mass spectra contain molecular ion peaks at *m/z* 951 for **15** and 937 for **16**. The formation of compounds **15** and **16** from **10** and **11** involves activation of the methylidene C−H bond followed by loss of one carbonyl ligand.

Compounds **17** and **18** have been characterized by elemental analysis, infrared, ^{1}H NMR, and mass spectroscopic data together with a single-crystal X-ray structure analysis for **17**. The molecular structure of **17** is depicted in Figure 4, crystal data are given in Table 1, and selected bond distances and angles are summarized in Table 5. The structure is based upon a triangular array of osmium atoms in which the

Scheme 6

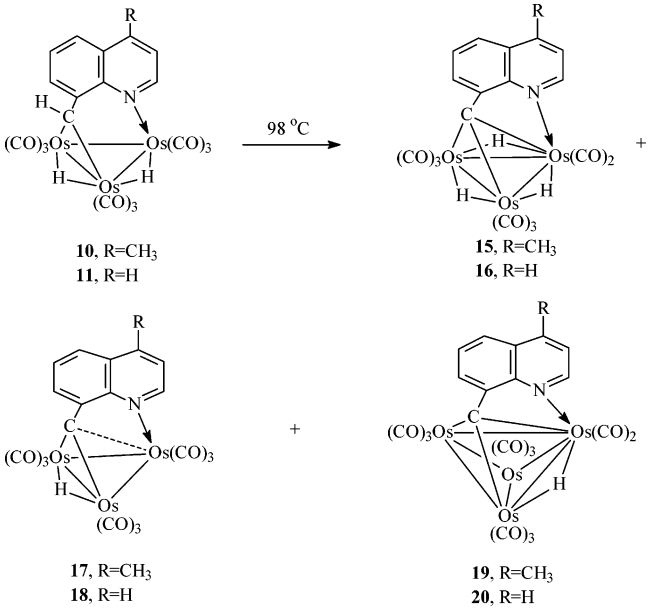

Table 5. Selected Bond Distances (Å) and Angles (deg) for 17

Bond Distances			
Os(1)−Os(2)	2.9077(9)	C(15)−C(19)	1.431(18)
Os(2)−Os(3)	2.8484(11)	C(16)−C(20)	1.505(18)
Os(1)−Os(3)	2.8230(10)	C(10)−C(11)	1.462(18)
Os(1)−C(10)	2.004(13)	C(11)−C(19)	1.44(2)
Os(2)−C(10)	2.038(13)	C(13)−C(14)	1.38(2)
Os(3)−C(10)	2.222(13)	C(15)−C(16)	1.399(19)
Os(3)−N(1)	2.199(10)	C(16)−C(17)	1.308(18)
C(11)−C(12)	1.357(17)	C(17)−C(18)	1.411(19)
C(12)−C(13)	1.407(18)	N(1)−C(19)	1.363(16)
C(14)−C(15)	1.452(18)	N(1)−C(18)	1.280(18)

Bond Angles			
Os(3)−Os(1)−Os(2)	59.59(2)	C(10)−Os(1)−Os(3)	51.5(4)
Os(3)−Os(2)−Os(1)	58.72(2)	C(10)−Os(3)−Os(2)	45.3(3)
Os(1)−Os(3)−Os(2)	61.68(3)	Os(1)−C(10)−Os(2)	92.0(5)
C(10)−Os(2)−Os(1)	43.5(4)	Os(1)−C(10)−Os(3)	83.6(5)
C(10)−Os(3)−Os(1)	44.9(3)	Os(2)−C(10)−Os(3)	83.8(5)
C(1)−Os(1)−Os(2)	117.6(4)	C(4)−Os(2)−Os(1)	117.9(4)

hydride-bridged Os(1)−Os(2) distance of 2.9077(9) Å is significantly longer than the other two Os−Os edges

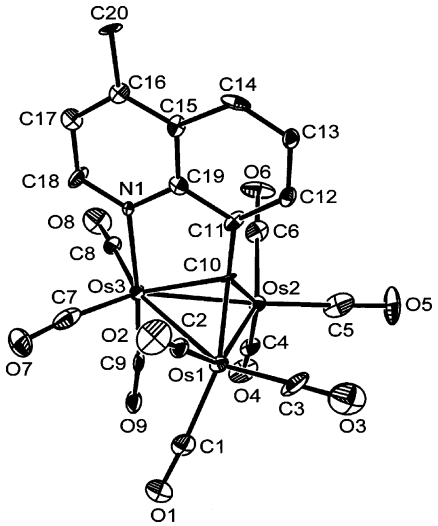

Figure 4. ORTEP drawing of (μ-H)$Os_3(CO)_9(\mu_3$-η^2-C(C_9H_5)-(4-CH_3)N), **17**. Thermal ellipsoids are drawn at the 50% probability level.

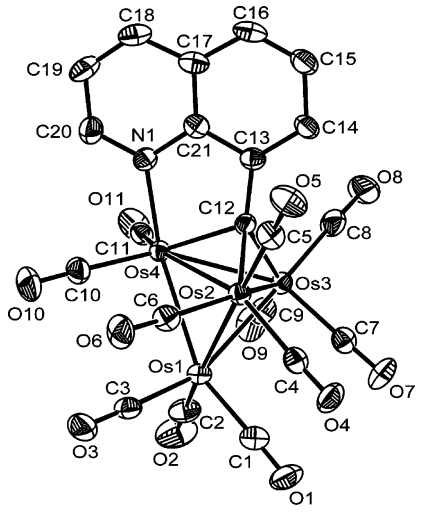

Figure 5. ORTEP drawing of (μ-H)$Os_4(CO)_{11}(\mu_3$-η^2-C(C_9H_6)N), **20**. Thermal ellipsoids are drawn at the 35% probability level.

(Os(1)−Os(3) = 2.8230(10) and Os(2)−Os(3) = 2.8484-(11) Å). The bridging hydride in **17** was not located crystallography but geometrically assigned to bridge the Os(1)−Os(2) edge according to the lengthening of the metal−metal vector. The most interesting feature of the structure of **17** is that the bridging heterocyclic ligand lies over the triosmium plane as reported for (μ-H)Os_3-$(CO)_{10}(\mu_3$-CR) (R = H, Ph, CH_2CHMe_2).[28−30] In the complex (μ-H)$Os_3(CO)_{10}(\mu_3$-CH) the CH ligand is closer to μ_3 and with the three Os−C distances being 2.35(1), 2.01(1), and 2.00(1) Å. In **17** the corresponding osmium−carbon distances are 2.222(13), 2.004(13), and 2.039(13) Å. These distances are indicative of some direct interaction between Os(3) and C(10), and hence this bonding mode may be termed as "semi-triply" bridging. Two additional electrons are donated by the N atom of the heterobicyclic ligand to Os(3) (Os(3)−N(1) = 2.199(10) Å), indicating a significant and direct bonding interaction between these two atoms. The spectroscopic data of **17** are consistent with its crystal structure. The close similarities of the IR and ^{1}H NMR spectra of **17** and **18** indicate that they have analogous structures.

The change in metal nuclearity associated with the formation of **19** and **20** indicates that cluster fragmentation and reaggregation processes are occurring. Crystals of **19** suitable for X-ray diffraction analysis could not be obtained, but suitable crystals of **20** have been obtained. The molecular structure of **20** is depicted in Figure 5, crystal data are given in Table 1, and selected bond lengths and angles are given in Table 6. The metal framework of **20** consists of a distorted Os_4 tetrahedron with Os−Os distances of Os(1)−Os(2) = 2.8199(4), Os(1)−Os(3) = 2.8148(4), Os(1)−Os(4) = 2.9011(4), Os(2)−Os(4) = 2.8549(4), Os(2)−Os(3) = 2.8435(4), and Os(3)−Os(4) = 2.8616(4) Å. The long Os(1)−Os(4) bond of 2.9011(4) Å is believed to contain the bridging hydride ligand which resonates at δ −21.50 but was not located crystallographically. This is sup-

(28) Shapley, J. R.; Uchiyama, M. E. C.; George, G. M. St.; Churchill, M. R.; Bueno, C. *J. Am. Chem. Soc.* **1983**, *105*, 140.
(29) Yeh, W.-Y.; Shapley, J. R.; Li, Y.; Churchill, M. R. *Organometallics* **1985**, *4*, 767.
(30) Green, M.; Orpen, A. G.; Schaverien, J. C. *J. Chem. Soc., Chem Commun.* **1984**, 37.1

Table 6. Selected Bond Distances (Å) and Angles (deg) for 20

Bond Distances			
Os(1)−Os(2)	2.8199(4)	C(18)−C(19)	1.363(14)
Os(2)−Os(3)	2.8435(4)	C(13)−C(14)	1.373(10)
Os(3)−Os(4)	2.8616(4)	C(14)−C(15)	1.432(11)
Os(2)−Os(4)	2.8549(4)	C(16)−C(17)	1.398(12)
Os(1)−Os(3)	2.8148(4)	C(17)−C(21)	1.417(11)
Os(1)−Os(4)	2.9011(4)	C(19)−C(20)	1.386(12)
Os(4)−N(1)	2.140(6)	N(1)−C(20)	1.341(10)
C(12)−C(13)	1.468(10)	N(1)−C(21)	1.375(10)
C(13)−C(21)	1.410(10)	C(13)−C(21)	1.410(10)
C(15)−C(16)	1.333(13)	C(15)−C(16)	1.333(13)
C(17)−C(18)	1.408(12)	C(17)−C(18)	1.408(12)
Bond Angles			
Os(2)−Os(1)−Os(4)	59.851(9)	C(12)−Os(2)−Os(3)	45.43(18)
Os(1)−Os(2)−Os(4)	61.486(9)	C(12)−Os(2)−Os(4)	46.70(19)
Os(1)−Os(3)−Os(2)	59.782(10)	C(12)−Os(3)−Os(1)	92.9(2)
Os(2)−Os(3)−Os(4)	60.054(9)	C(12)−Os(3)−Os(2)	46.54(19)
Os(3)−Os(1)−Os(2)	60.614(10)	C(12)−Os(3)−Os(4)	46.62(19)
Os(3)−Os(1)−Os(4)	60.063(10)	C(12)−Os(2)−Os(4)	46.7(2)
Os(1)−Os(2)−Os(3)	59.604(10)	C(12)−Os(4)−Os(2)	46.25(19)
Os(3)−Os(2)−Os(4)	60.288(9)	C(12)−Os(4)−Os(3)	45.07(18)
Os(1)−Os(3)−Os(4)	61.464(10)	Os(3)−C(12)−Os(2)	88.0(3)
Os(2)−Os(4)−Os(1)	58.663(10)	Os(3)−C(12)−Os(4)	88.3(3)
Os(2)−Os(4)−Os(3)	59.658(9)	Os(2)−C(12)−Os(4)	87.0(3)
Os(3)−Os(4)−Os(1)	58.473(10)	C(12)−Os(4)−N(1)	76.6(2)
C(12)−Os(2)−Os(1)	91.95(19)		

ported by the CO ligand displacements observed around these coordination sites. The bridging tertiary carbon C(12) donates three electrons to the metal core through similar metal−carbon σ-bonds to Os(2), Os(3), and Os(4) (C(12)−Os(2) = 2.065(7), C(12)−Os(3) = 2.027(6), and C(12)−Os(4) = 2.081(7) Å). This is in sharp contrast to **17**, and when taken together with the almost equal Os−Os bond lengths of the carbon-capped face, suggests a much more symmetrical bonding interaction resulting from capping the opposite face with the fourth osmium atom. The metal atoms Os(1), Os(2), and Os(3) each contain three linear carbonyl ligands, and the other metal atom Os(4) has only two. Two additional electrons are donated by the lone pair on nitrogen via a two-electron donor σ-bond from N(1) to Os(4). The Os(4)−N(1) bond length in **20** (2.140(6) Å) is very similar to the Os(2)−N(1) bond lengths in **6** (2.13(2) Å).[23a] As far as electron counting is concerned, cluster **20** contains 60 cluster valence electrons (CVE) and is consistent with the six metal−metal bonds observed in the structure in accord with the effective atomic number (EAN) rule. The spectroscopic properties of **20** are consistent with the solid-state structure. The infrared and ^{1}H NMR spectroscopic data of **20** are very similar to those of **19**, indicating that they have analogous structures.

A similar thermolysis of **10** and **11** but at 80 °C and in the presence of H_2 (1 atm) gives the trihydrides **15** and **16** in 72 and 77% yields, respectively, in addition to trace amounts of the parent clusters **6** and **7**. The spectroscopic properties of **20** are consistent with the solid-state structure. The infrared and ^{1}H NMR spectroscopic data of **20** are very similar to those of **19**, indicating that they have analogous structures.

In contrast to the thermolysis of **10** and **11**, which afforded a mixture of two trinuclear complexes and one tetranuclear complex, the thermolysis of **12** and **13** proceeds smoothly to yield (μ-H)$Os_3(CO)_9(\mu_3$-η^2-CC_8H_4-(5-CH_3)N_2) (**21**) and (μ-H)$Os_3(CO)_9(\mu_3$-η^2-$C(C_8H_5N_2)$) (**22**), respectively (Scheme 7). The infrared and ^{1}H NMR

Scheme 7

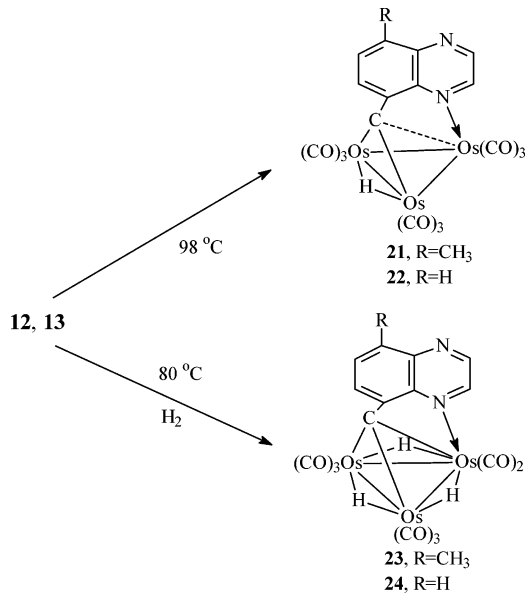

Table 7. Reduction Potential of Compounds in CH_2Cl_2 Relative to Fc/Fc^+

compound	reduction in volts
10	−2.24 (E_{IRR})
12	−1.60 (E_{REV})
13	−1.64 (E_{REV})
23	−1.74 (E_{REV})
24	−1.65 (E_{REV})
25	−1.63 (E_{REV})

spectra and of **21** and **22** are virtually identical to those observed for **17** and **18**, indicating that they are structurally similar. The formulations of **21** and **22** are clear from their mass spectra, which show molecular ion peaks at *m/z* 978 for **21** and 964 for **22**.

The thermolysis of **12** and **13** in the presence of molecular hydrogen (1 atm) at 80 °C gives the trihydrides (μ-H)$_3Os_3(CO)_8(\mu_3$-η^2-CC_8H_4(5-CH_3)N_2) (**23**) and (μ-H)$_3Os_3(CO)_8(\mu_3$-η^2-$CC_8H_5N_2$) (**24**), respectively, in high yields. Both compounds have been characterized by elemental analysis, infrared, and ^{1}H NMR spectroscopy. The infrared spectra of **23** and **24** are very similar to those of **15** and **16** and (μ-H)$_3Os_3(CO)_8(\mu_3$-η^2-CHC_7H_3-(Me)NS), indicating that they are isostructural.

Electrochemical studies of the methylidene insertion cluster containing the quinoxaline ligand are of interest due to the interesting electrochemical behavior observed from our previous studies of the quinoxaline ligand and quinoxaline triosmium clusters.[25] The quinoxaline containing a 48-electron precise cluster, (μ-H)$Os_3(CO)_{10}(\mu$-η^2-$C_8H_5N_2$), showed a one-electron reversible reduction potential at −1.63 V vs Fc/Fc^+. This reduction potential is significantly less negative than the free ligand, and the latter is also irreversible.[25] Very similar electrochemical behavior is observed for the diazomethane reaction products. The electrochemical reduction potentials of the complexes are provided in Table 7. The quinoxaline-containing complexes **12**, **13**, **23**, and **24** all show reversible one-electron reduction potentials at −1.70, −1.64, −1.74, and −1.65 V in CH_2Cl_2 vs Fc/Fc^+, respectively, whereas the quinoline derivative **10** shows an irreversible reduction at −2.24 V. The reversibility of the CVs for **12**, **13**, **23**, and **24** was gauged on the

Table 8. Selected Calculated Bond Angles and Bond Lengths for 12 and 13

Bond Distances

12				13			
Os(1)−Os(2)	3.08	C(12)−C(17)	1.45	Os(1)−Os(2)	2.855	C(10)−C(11)	1.480
Os(2)−Os(3)	2.90	C(13)−C(14)	1.38	Os(2)−Os(3)	3.080	C(11)−C(18)	1.440
Os(1)−Os(3)	2.85	C(13)−C(18)	1.50	Os(1)−Os(3)	2.90	C(13)−C(14)	1.370
Os(1)−C(19)	2.17	C(14)−C(15)	1.40	Os(1)−C(10)	2.170	C(15)−C(18)	1.45
Os(3)−C(19)	2.18	C(15)−C(16)	1.40	Os(3)−C(10)	2.180	C(11)−C(12)	1.40
Os(2)−N(1)	2.23	C(16)−C(17)	1.43	N(1)−C(17)	1.340	C(12)−C(13)	1.40
C(10)−C(11)	1.40	C(16)−C(19)	1.48	N(2)−C(16)	1.320	C(14)−C(15)	1.41
C(11)−N(2)	1.32	C(17)−N(1)	1.39	N(1)−C(18)	1.390	C(16)−C(17)	1.40
C(12)−N(2)	1.36	C(12)−C(13)	1.42	N(2)−C(15)	1.37		
C(10)−N(1)	1.34						

Bond Angles

12		13	
Os(3)−Os(2)−Os(1)	58.32	Os(1)−Os(2)−Os(3)	58.37
Os(2)−Os(3)−Os(1)	64.81	Os(2)−Os(1)−Os(3)	64.81
Os(3)−Os(1)−Os(2)	56.85	Os(1)−Os(3)−Os(2)	56.80
C(5)−Os(2)−Os(1)	113.67	C(3)−Os(1)−Os(2)	92.85
N(1)−Os(2)−Os(3)	90.46	C(2)−Os(1)−Os(2)	93.11
C(1)−Os(1)−Os(3)	94.73	C(2)−Os(1)−Os(3)	120.34
C(8)−Os(3)−Os(1)	120.31	N(1)−Os(2)−Os(1)	90.36
C(3)−Os(1)−Os(2)	110.78	Os(1)−C(10)−Os(3)	83.50
C(19)−Os(3)−Os(1)	48.17	C(1)−Os(1)−Os(2)	167.61
C(19)−Os(1)−Os(3)	46.33	C(10)−Os(1)−Os(2)	81.29
Os(3)−C(19)−Os(1)	83.49	C(1)−Os(1)−Os(3)	102.88
		C(10)−Os(1)−Os(3)	48.31
		C(5)−Os(2)−N(1)	88.38
		C(6)−Os(2)−Os(1)	171.53
		C(10)−Os(3)−Os(1)	48.17
		C(10)−Os(3)−Os(2)	75.89

criteria that the half-wave potentials of the reductive and oxidative scans were separated by less than 80 mV at scan rates of 200 mV/s. The similar reduction potentials of the quinoxaline-containing 48-electron cluster, (μ-H)$Os_3(CO)_{10}$(μ-η^2-$C_8H_5N_2$) (**25**), **13**, and **24** suggest that the binding mode of the heterocycle to the metal cluster has little effect on their reduction potentials. This is in agreement with our previously reported DFT calculations, which showed that the LUMO is predominantly ligand based for the previously studied (μ-H)$Os_3(CO)_{10}$(μ-η^2-$C_8H_5N_2$).[25] The methyl substitutent on the quinoxaline ring shifts the reduction potential about 60−90 mV toward more negative potential due to the expected electron-donating effect of the methyl group. It would appear that the cluster acts as an electron sink for the bonding electrons of the heterocycle, delocalizing them onto the core and the carbonyl ligands, and that this delocalization takes place whether the C(8) carbon of the quinoxaline ring is directly bound to the metal or connected through a methylidene or methylidyne carbon with concomitant stabilization of the LUMO. The relatively short C−C distances between C(8) and these carbons implies some conjugation with the ring in these systems (1.489 and 1.497 Å). This effect is large enough to sufficiently stabilize the radical anions of the more electron-poor heterocycle quinoxaline and makes the reductions reversible. This is not the case for the relatively more electron-rich quinolines.

Density functional theory calculations were carried out on complexes **12** and **13**. The optimized geometries gave bond lengths and angles that are in good agreement with the experimentally determined bond lengths for **12** and **13** (Tables 4, 5, and 8). Spin density calculations on the corresponding radical anions reveal that most of the spin density is distributed within the ring at the two nitrogen atoms and at positions 2, 3, and 5 of the ring (scaled to 1000 for $1e^-$, Figure 7). The net natural charge population analysis (NPA) of the C−H groups on the heterocyclic ring of **12** and **13** reveals localization of the most positive charges at the C-2 and C-3 position (Figure 7). There is also a significant amount of positive charge distributed on the carbonyl of Os(1) and particularly at the axial carbonyl of Os(2) for **12**. Similar charge distribution patterns were also found for compound **13**. The charge distributions at the C-2 and C-3 position are very similar. However, the spin density calculation shows that more spin density is localized at C-2 rather than at C-3 position. Another interesting feature is found at the C-5 position, which has a net charge very similar to the C-6 or C-7 positions but where significant spin density is found, suggesting particular stabilization of the resulting radical anion probably due to its *para*-relationship to the cluster-bound carbon atom which can delocalize bonded electrons to the cluster. Most importantly, in general the higher the positive charge at a particular position, the higher the calculated spin density at that

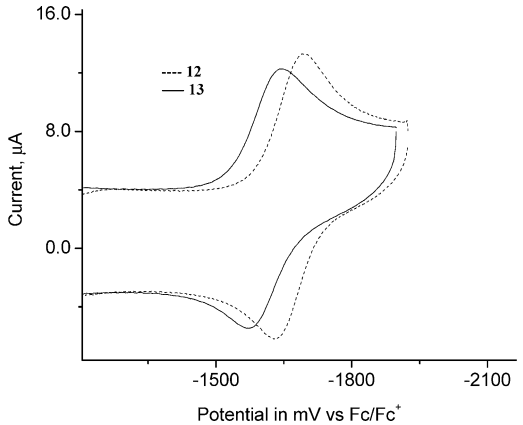

Figure 6. Cyclic voltammogram of **12** and **13** at 400 mV/s vs Fc/Fc^+.

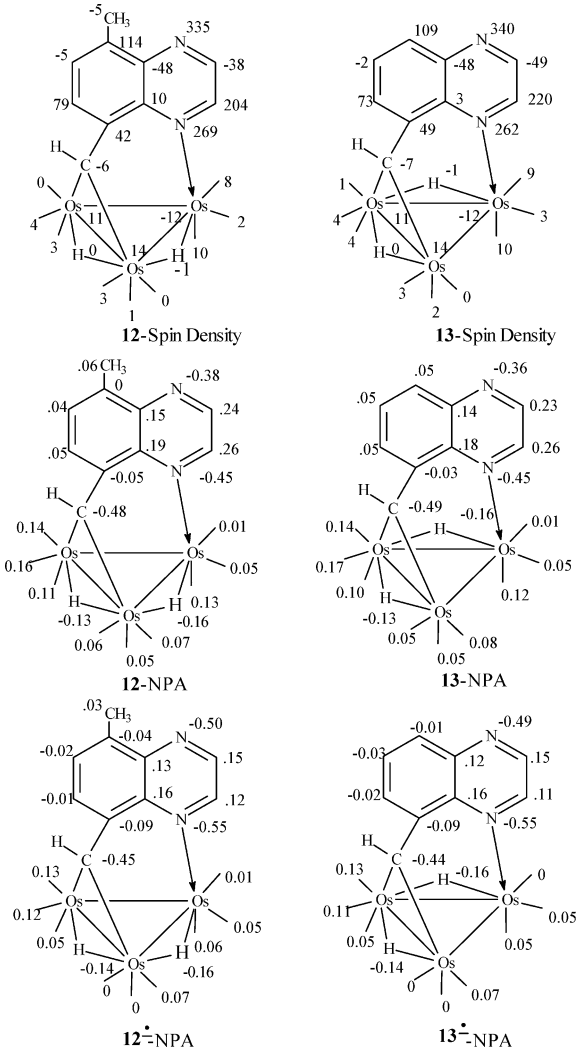

Figure 7. Distribution of spin density and natural charge in **12** and **13**. Sum of the natural charges of C and O and C and H are shown on the CO groups and on the benzoheterocycle, respectively.

position (Figure 7). The natural charge analysis of radicals **12** and **13** shows that the natural charges at C-2 and on the nitrogen atoms are shifted significantly toward more negative values than on any other atoms. Notably the carbonyl carbons do not show nearly the same change in net charge consistent with the idea that most of the charge due to the added electron remains in the heterocycle. The stabilities of the radicals of these complexes on the cyclic voltammetry time scale are thus mainly due to the distribution of unpaired spin density into the heterocyclic ring, and this explains the difference in behavior between quinoline and quinoxaline. The rather narrow range in measured reduction potentials observed for **12**, **13**, and **23**−**25** relative to the diversity in bonding modes of **12** and **13** versus **23**, **24**, and **25** is surprising and is not reflected in the NPA analyses.

Conclusions

The reaction of the quinoxaline triosmium cluster **8** with diazomethane represents a novel example of insertion of one methylene group into the Os−C σ-bond of the cluster and another to the C(5)−H bond of the carbocyclic ring, resulting in modification of the heterocyclic ligand and affording compound **12** (Scheme 4). Thus, the now well-known attack of nucleophiles at the C(5) of quinoline in these electron-deficient clusters is paralleled by diazomethane (commonly viewed as an electrophile), but only in the case of the more electron-deficient quinoxaline system does substitution of methyl for hydrogen at the 5 position redirect the reaction toward the Os−C and Os−H bonds to give **12** and **14**. The latter provides a second interesting example of a triosmium cluster containing an edge-bridging methylene group and a σ-bound methyl group.[21]

Compounds **10** and **11**, on thermolysis, produce one tetranuclear and two trinuclear complexes (Scheme 6), while **12** and **13** give only a single monohydrido triosmium compound which corresponds to only one of the three compounds obtained from **10** and **11**. This may also be related to the more electron-poor quinoxaline ring system.

In summary, the reactivity of diazomethane toward unsaturated triosmium clusters containing heterocyclic ligands is markedly influenced by the structure of the ligand. To explore the effect of the structure of the diazoalkane on product formation, investigations of the reactivity of **1**, **4**, and **6**−**9** with diphenyldiazomethane, dimethyldiazomethane, and diazoacetate are currently underway in our laboratories. Finally, it is interesting to note that the binding of the electron-poor quinoxaline ring to the cluster in a variety of bonding modes gives clusters capable of one-electron reversible reduction, whereas the free ligand shows irreversible reduction at more negative potentials. It would appear that coordination of the heterocycle to the osmium core in almost any bonding arrangement is sufficient to stabilize radical anions on the cyclic voltammetry time scale relative to the free ligand. This is only true, however, for electron-precise clusters with relatively electron-poor heterocycles. The natural charge population analysis and spin density calculations also demonstrate that charge localization in the heterocyclic ring is the primary origin of the radical stabilities of compounds **12** and **13**.

Experimental Section

General Procedures. Although the reaction products are air stable, all of the reactions were performed under an atmosphere of nitrogen. Reagent grade solvents were freshly distilled from appropriate drying agents. Infrared spectra were recorded on a Shimadzu FTIR 8101 spectrophotometer. NMR spectra were recorded on Varian Unity Plus 400 and Bruker DPX 400 instruments. Elemental analyses were performed by Schwarzkopf Microanalytical Laboratories, Woodside, NY. The compounds (μ-H)$Os_3(CO)_9(\mu_3$-η^2-C_9H_5(4-CH_3)N) (**6**), (μ-H)Os_3-$(CO)_9(\mu_3$-η^2-C_9H_6N) (**7**), (μ-H)$Os_3(CO)_9(\mu_3$-η^2-$C_8H_5N_2$) (**8**), and (μ-H)$Os_3(CO)_9(\mu_3$-η^2-C_8H_4(5-CH_3)N_2) (**9**) were prepared according to the published procedures.[23a,d] Diazomethane was prepared from diazald (*N*-methyl-*N*-nitroso-*p*-toluenesulfonamide) using an Aldrich mini diazald apparatus.

Reaction of (μ-H)$Os_3(CO)_9(\mu_3$-η^2-C_9H_5)(4-CH_3)N) (6) with CH_2N_2. An ethereal solution of freshly prepared diazomethane (~0.700 g, ~16.6 mmol) was added to a dichloromethane solution (10 mL) of **3** (0.155 g, 0.160 mmol) at 0 °C, and the reaction mixture was warmed to room temperature. Immediate formation of insoluble polymethylene was observed. The reaction mixture was stirred at room temperature for 1 h, during which time the color changed from green to yellow. The

polymer was separated by filtration, and the solvent from the filtrate was removed under reduced pressure. The residue was chromatographed by TLC on silica gel. Elution with hexane/CH_2Cl_2 (5:1, v/v) gave one major band, which afforded (μ-H)$_2$Os$_3$(CO)$_9$(μ_3-η^2-CH(C$_9$H$_5$)(4-CH$_3$)N) (**10**) (0.125 g, 80%) as yellow crystals after recrystallization from hexane/CH_2Cl_2 at −20 °C. Anal. Calcd for $C_{20}H_{11}NO_9Os_3$: C, 24.51; H, 1.13; N, 1.43. Found: C, 24.65; H, 1.24; N, 1.45. IR (νCO, hexane): 2092s, 2066vs, 2039vs, 2005m, 1986m, 1963w, 1939w cm^{-1}. ^{1}H NMR ($CDCl_3$): δ 2.68 (s, 3H), 6.62 (d, 1H, J = 2.0 Hz), 6.99 (d, 1H, J = 5.2 Hz), 7.29 (dd, 1H, J = 7.4, 1.6 Hz), 7.66 (d, 1H, J = 7.6 Hz), 7.84 (d, 1H, J = 6.8 Hz), 9.53 (d, 1H, J = 5.2 Hz) −14.76 (d, 1H, J = 2.0 Hz) −15.16 (t, 1H, J = 2.0 Hz). ^{13}C{^{1}H} NMR ($CDCl_3$), carbonyl region: δ 166.4 (s, 1C), 171.4 (s, 1C), 171.8 (s, 1C), 173.0 (s, 1C), 173.8(s, 1C), 174.5(s, 1C), 177.2 (s, 1C), 179.9 (s, 1C), and 184.1 (s, 1C); hydrocarbon region: δ 20.3(s, 1C), 41.0 (s, 1C), 119.9 (s, 1C), 122.3 (s, 1C), 127.5 (s, 1C), 131.0 (s, 1C), 131.8 (s, 1C), 146.2 (s, 1C), 149.7 (s, 1C), 158.4 (s, 1C), and 162.6 (s, 1C). MS: (*m/z*) 979 [M]$^+$.

Reaction of (μ-H)Os$_3$(CO)$_9$(μ_3-η^2-C$_9$H$_6$)N) (7) with CH_2N_2. A reaction similar to that above of an ethereal solution of freshly prepared CH_2N_2 (∼0.700 g, ∼16.6 mmol) with **7** (0.145 g, 0.150 mmol) followed by similar chromatographic workup gave one major band, which afforded (μ-H)$_2$Os$_3$(CO)$_9$(μ_3-η^2-CH-(C$_9$H$_6$)N) (**11**) (0.125 g, 85%) as yellow crystals after recrystallization from hexane/CH_2Cl_2 at −20 °C. Anal. Calcd for $C_{19}H_9NO_9Os_3$: C, 23.62; H, 0.94; N, 1.45. Found: C, 23.83; H, 1.05, N, 1.54. IR (νCO, hexane): 2094m, 2067s, 2044vs, 2010vs, 1993m, 1988m, 1974w, 1968m cm^{-1}. ^{1}H NMR ($CDCl_3$): δ 6.58 (d, 1H, J = 2.0 Hz), 7.14 (dd, 1H, J = 5.2, 8.4 Hz), 7.31(t, 1H, J = 7.0 Hz), 7.49 (dd, 1H, J = 1.4, 7.0 Hz), 7.87 (d, 1H, J = 7.6 Hz), 8.28 (dd, 1H, J =1.4, 8.0 Hz), 9.68 (dd, 1H, J = 1.4, 5.2 Hz), −14.74 (d, 1H, J = 2.0 Hz), −15.21 (t, 1H, J = 2.0 Hz). MS: (*m/z*) 965 [M]$^+$.

Reaction of (μ-H)Os$_3$(CO)$_9$(μ_3-η^2-C$_8$H$_5$N$_2$) (8) with CH_2N_2. A treatment similar to that above of **8** (0.095 g, 0.098 mmol) with CH_2N_2 (∼0.700 g, ∼16.6 mmol) at 0 to 25 °C for 1.5 h followed by similar chromatographic separation gave the following compounds in order of elution. (μ-H)$_2$Os$_3$(CO)$_9$(μ_3-η^2-CH(C$_8$H$_4$)(5-CH$_3$)N$_2$) (**12**) (0.019 g, 20%) as red crystals from hexane/CH_2Cl_2 at −20 °C: Anal. Calcd for $C_{19}H_{10}N_2O_9Os_3$: C, 23.26; H, 1.03; N, 2.86. Found: C, 23.38; H, 1.15; N, 2.92. IR (νCO, CH_2Cl_2): 2094m, 2969vs, 2042vs, 2004s, 1992m, 1967m, cm^{-1}. ^{1}H NMR (CD_2Cl_2): δ 9.56 (d, 1H, J = 2.8 Hz), 8.59 (d, 1H, J = 2.8 Hz), 7.87 (d, 1H, J = 7.6 Hz), 7.44 (d, 1H, J = 7.6 Hz), 6.54 (d, 1H, J = 1.6 Hz), 2.58 (s, 3H), −14.69 (d, 1H, J = 1.6 Hz), −15.19 (t, 1H, J = 1.6 Hz). ^{13}C{^{1}H} NMR (CD_2Cl_2), carbonyl region: δ 171.8 (s, 1C), 171.9 (s, 1C), 173.3 (s, 1C), 173.9 (s, 1C), 174.5 (s, 1C), 177.5 (s, 1C), 180.3 (s, 1C), 182.8 (s, 1C), 183.6 (s, 1C); hydrocarbon region: δ 17.8 (s, 1C), 39.8 (s, 1C), 130.9 (s, 1C), 132.2 (s, 1C), 133.6 (s, 1C), 143.2 (s, 1C), 150.3 (s, 1C), 157.7 (s, 1C), 160.9 (s, 1C), 166.5 (s, 1C). MS: *m/z* 980. (μ-H)$_2$Os$_3$(CO)$_8$(μ_3-η^2-CHC$_8$H$_5$N$_2$), **13** (0.033 g, 35%), as red crystals after recrystallization from hexane/CH_2Cl_2 −20 °C: Anal. Calcd for $C_{18}H_8N_2O_9Os_3$: C, 22.36; H, 0.84; N, 2.90. Found: C, 22.48; H, 0.97; N, 2.96. IR (νCO, CH_2Cl_2): 2096m, 2070vs, 2042vs, 2010s, 1992s, 1967m cm^{-1}. ^{1}H NMR (CD_2Cl_2): δ 9.51(d, 1H, J = 3.2 Hz), 8.57 (d, 1H, J = 3.2 Hz), 7.95 (dd, 1H, J = 7.6, 1.2 Hz), 7.85 (dd, 1H, J = 7.6, 1.2 Hz), 7.54 (t, 1H, J = 7.6 Hz), 6.47 (d, 1H, J = 1.6 Hz), −14.70 (d, 1H, J = 1.6 Hz), −15.24 (t, 1H, J = 1.6 Hz). MS: *m/z* 966.

Reaction of (μ-H)Os$_3$(CO)$_9$(μ_3-η^2-C$_8$H$_4$(5-CH$_3$)N$_2$) (9) with CH_2N_2. A similar reaction of **9** (0.095 g, 0.098 mmol) with diazomethane (0.700 g, 16.6 mmol) at 0 to 25 °C followed by similar chromatographic separation afforded **12** (0.047 g, 49%) and Os$_3$(CO)$_9$(μ-η^2-C$_8$H$_4$(5-CH$_3$)N$_2$)(μ-CH$_2$)CH$_3$ (**14**) (0.011 g, 11%) as orange crystals from hexane/CH_2Cl_2 at −5 °C. Anal. Calcd for $C_{20}H_{12}N_2O_9Os_3$: C, 24.14; H, 1.22; N, 2.82. Found: C, 24.48; H, 1.34; N, 2.88. IR (νCO, CH_2Cl_2): 2095m, 2068vs, 2041vs, 2009s, 1988s, 1962w cm^{-1}. ^{1}H NMR (CD_2Cl_2): δ 8.80 (d, 1H, J = 2.4 Hz), 8.61 (d, 1H, J = 2.4 Hz), 8.57 (d, 1H, J = 7.2 Hz), 7.50 (d, 1H, J = 7.2 Hz), 7.40 (d, 1H, J = 6.8 Hz), 6.27 (d, 1H, J = 6.8 Hz), 2.66 (s, 3H), 0.76 (s, 3H).

Thermolysis of 10. A heptane solution (20 mL) of **10** (0.100 g, 0.102 mmol) was heated to reflux for 2.5 h. The solvent was removed in vacuo and the residue subjected to TLC on silica gel. Elution with hexane/CH_2Cl_2 (5:1, v/v) gave four bands. The fast band gave (μ-H)$_3$Os$_3$(CO)$_8$(μ_3-η^2-C(C$_9$H$_5$)(4-CH$_3$)N) (**15**) (0.016 g, 17%) as pale yellow crystals after recrystallization from hexane/CH_2Cl_2 at −20 °C. Anal. Calcd for $C_{19}H_{11}NO_8Os_3$: C, 23.97; H, 1.17; N, 1.47. Found: C, 23.75; H, 1.08; N, 1.28. IR (νCO, CH_2Cl_2): 2093m, 2074s, 2018m, 2014vs, 1987w, 1954m cm^{-1}. ^{1}H NMR ($CDCl_3$): δ 8.96 (d, 1H, J = 4.8 Hz), 7.82 (d, 1H, J = 6.6 Hz), 7.25(dd, 1H, J = 6.6, 4.8 Hz), 7.52 (t, 1H, J = 4.8 Hz), −17.11(t, 1H, J = 2.2 Hz), −18.08 (t, 1H, J = 2.2 Hz), −18.81 (t, 1H, J = 2.2 Hz). MS: (*m/z*) 951 [M]$^+$. The second band afforded (μ-H)Os$_3$(CO)$_9${μ_3-η^2-C(C$_9$H$_5$)-(4-CH$_3$)N) (**17**) (0.030 g, 30%) as orange crystals from hexane/CH_2Cl_2 at −20 °C. Anal. Calcd for $C_{20}H_9NO_9Os_3$: C, 24.56; H, 0.93; N, 1.43. Found: C, 24.62; H, 1.02; N, 1.58. IR (νCO, hexane): 2085m, 2058vs, 2029vs, 2008s, 1987m, 1979w, 1962w cm^{-1}. ^{1}H NMR ($CDCl_3$): δ 2.65 (s, 3H), 7.06 (d, 1H, J = 4.8 Hz), 7.43 (d, 1H, J = 6.4 Hz), 7.52 (dd, 1H, J = 7.6, 1.4 Hz), 7.79 (d, 1H, J = 6.0 Hz), 9.30 (d, 1H, J = 4.8 Hz),-16.66 (s, 1H). MS: (*m/z*) 977 [M]$^+$. The third band gave a trace amount of an uncharacterized compound. The fourth band gave (μ-H)-Os$_4$(CO)$_{11}$(μ_3-η^2-C(C$_9$H$_5$)(4-CH$_3$)N) (**19**) (0.019 g, 15%) as red crystals after recrystallization from hexane/CH_2Cl_2 at −20 °C. Anal. Calcd for $C_{20}H_9NO_9Os_3$: C, 24.56; H, 0.93; N, 1.43. Found C, 21.65; H, 0.92; N, 1.28. IR (νCO, hexane): 2085m, 2081s 2056m, 2039vs, 2025s, 1980m cm^{-1}. ^{1}H NMR ($CDCl_3$): δ 2.69-(s, 3H), 7.15 (d, 1H, J = 4.8 Hz), 7.81 (t, 1H, J = 7.6), 8.06 (d, 1H, J = 7.4 Hz), 8.56 (d, 1H, J = 7.2 Hz), 9.22 (d, 1H, J = 5.2 Hz), −21.46 (s, 1H). MS: (*m/z*) 1224 [M]$^+$.

Thermolysis of 11. A heptane solution (20 mL) of **11** (0.075 g, 0.078 mmol) was heated to reflux for 2.5 h. The solvent was removed in vacuo, and the residue was subjected to TLC on silica gel. Elution with hexane/CH_2Cl_2 (5:1, v/v) gave four bands. The fast band gave (μ-H)$_3$Os$_3$(CO)$_8$(μ_3-η^2-C(C$_9$H$_6$)N) (**16**) (0.011 g, 15%) as pale yellow crystals after recrystallization from hexane/CH_2Cl_2 at −20 °C. Anal. Calcd for $C_{18}H_9NO_8Os_3$: C, 23.05; H, 0.97; N, 1.49. Found: C, 23.27; H, 1.15; N, 1.51. IR (νCO, CH_2Cl_2): 2094m, 2074vs, 2019s, 2013vs, 2007w, 1986w, 1955m, cm^{-1}. ^{1}H NMR ($CDCl_3$): δ 7.12 (dd, 1H, J = 7.2, 1.2 Hz), 7.30 (t, 1H, J = 7.2 Hz), 7.48 (m, 2H), 8.14 (dd, 1H, J = 7.8, 1.2 Hz), 9.12 (d, 1H, J = 5.8 Hz), −16.98 (t, 1H, J = 2.0 Hz), −18.10 (t, 1H, J = 2.0 Hz), −18.65 (t, 1H, J = 2.0 Hz). MS: (*m/z*) 937 [M]$^+$. The second band afforded (μ-H)Os$_3$-(CO)$_9$(μ_3-η^2-C(C$_9$H$_6$)N) (**18**) (0.027 g, 36%) as orange crystals from hexane/CH_2Cl_2 at −20 °C. Anal. Found: C, 23.78; H, 0.89; N, 1.57. $C_{19}H_7NO_9Os_3$: C, 23.67; H, 0.73; N, 1.45. IR (νCO, hexane): 2085m, 2057vs, 2029vs, 2009s, 1988m, 1979w, 1963w, cm^{-1}. ^{1}H NMR ($CDCl_3$): δ 7.22 (m, 2H), 7.44 (t, 1H, J = 8.0 Hz), 7.49 (t, 1H, J = 7.6 Hz), 8.26 (dd, 1H, J = 8.4, 1.2 Hz), 9.22 (d, 1H, J = 6.4 Hz), −16.61 (s, 1H). MS (*m/z*) 963 [M]$^+$. The third band was too small for complete characterization, while the fourth band gave (μ-H)Os$_4$(CO)$_{11}$(μ_3-η^2-C(C$_9$H$_6$)N) (**20**) (0.017 g, 18%) as red crystals after recrystallization from hexane/CH_2Cl_2 at −20 °C. Anal. Found: C, 20.96; H; 0.69, N, 1.29. $C_{21}H_7NO_{11}Os_4$: C, 20.84; H, 0.58; N, 1.16. IR (νCO, CH_2Cl_2): 2080s, 2060vs, 2037m, 2022s, 1989s, cm^{-1}. ^{1}H NMR ($CDCl_3$): δ 2.69 (s, 3H), 7.15 (d, 1H, J = 4.8 Hz), 7.81 (t, 1H, J = 7.6 Hz), 8.06 (d, 1H, J = 7.4 Hz), 8.56 (d, 1H, J = 7.2 Hz), 9.22 (d, 1H, J = 5.2 Hz), −21.46 (s, 1H). MS: (*m/z*) 1210 [M]$^+$.

Thermolysis of 10 in the Presence of H_2. A cyclohexane solution (50 mL) of **10** (0.105 g, 0.109 mmol) was heated to reflux under hydrogen (1 atm) for 8 h. The solvent was removed under reduced pressure and the residue chromatographed by TLC on silica gel. Elution with hexane/CH_2Cl_2 (10:

3, v/v) gave, in order of elution, **15** (0.073 g, 72%) and **6** (0.011 g, 11%).

Thermolysis of 11 in the Presence of H_2. A similar thermolysis of **11** (0.075 g, 0.078 mmol) followed by similar chromatographic separation gave **16** (0.056 g, 77%) and **7** (0.008 g, 11%).

Thermolysis of 13. A heptane solution (20 mL) of **13** (0.033 g, 0.034 mmol) was heated to reflux for 2 h. The solvent was removed under reduced pressure, and the residue was chromatographed by TLC on silica gel. Elution with hexane/CH_2Cl_2 (3:2, v/v) developed two bands. The first band gave (μ-H)$Os_3(CO)_9(\mu_3$-η^2-C($C_8H_5N_2$) (**22**) (0.012 g, 36%) as red crystals from hexane/CH_2Cl_2 at −20 °C. Anal. Calcd for $C_{18}H_6N_2O_9Os_3$: C, 22.41; H, 0.63; N, 2.90. Found: C, 22.68; H; 0.45, N, 2.96. IR (νCO, CH_2Cl_2): 2087m, 2058vs, 2031s, 2004m, 1992m, 1983w cm^{-1}. ^{1}H NMR ($CDCl_3$): δ 9.18 (d, 1H, J = 2.4 Hz), 8.76 (dd, 1H, J = 6.6, 1.4 Hz), 8.70 (dd, 1H, J = 8.4, 1.4 Hz), 8.57 (d, 1H, J = 2.4 Hz), 7.48 (t, 1H, J = 6.8 Hz), −16.45 (s, 1H). MS: (*m/z*) 964 [M]$^+$. The second band was too small for complete characterization.

Thermolysis of 12. A similar thermolysis of **12** (0.033 g, 0.034 mmol) in heptane (20 mL) for 2 h followed by similar workup gave (μ-H)$Os_3(CO)_9\{\mu_3$-η^2-CC_8H_4(5-CH_3)N_2) (**21**) (0.014 g, 42%) as red crystals after recrystallization from hexane/CH_2Cl_2 at 0 °C. Anal. Calcd for $C_{19}H_{10}N_2O_9Os_3$: C, 23.26; H, 1.03; N, 2.86. Found: C, 23.35; H, 1.15; N, 2.92. IR (νCO, CH_2Cl_2): 2085m, 2058vs, 2031vs, 2006s, 1981s cm^{-1}. ^{1}H (NMR, CD_2Cl_2): δ 9.21 (d, 1H, J = 2.4 Hz), 8.69 (d, 1H, J = 2.4 Hz), 7.62 (d, 1H, J = 7.2 Hz), 7.43 (d, 1H, J = 7.2 Hz), 2.65 (s, 3H), −16.43 (s, 1H). MS: (*m/z*) 978 [M]$^+$.

Thermolysis of 12 in the Presence of H_2. A cyclohexane solution (50 mL) of **12** (0.085 g, 0.087 mmol) was refluxed under hydrogen (1 atm) for 8 h. The solvent was removed under reduced pressure and the residure chromatographed by TLC on silica gel. Elution with hexane/CH_2Cl_2 (1:1, v/v) gave one major band, which afforded (μ-H)$_3Os_3(CO)_8(\mu_3$-η^2-CC_8H_4-(5-CH_3)N_2) (**23**) (0.072 g, 87%) as red crystals after recrystallization from hexane/CH_2Cl_2 at −20 °C. Anal. Calcd for $C_{18}H_{10}N_2O_8Os_3$: C, 22.69; H, 1.06; N, 2.94. Found: C, 22.89; H, 1.18; N, 2.98. IR (νCO, CH_2Cl_2): 2090m, 2072vs, 2017m, 2013s, 1985s, 1951m cm^{-1}. ^{1}H (NMR, $CDCl_3$): δ 9.05 (d, 1H, J = 2.4 Hz), 8.75 (d, 1H, J = 2.4 Hz), 7.77 (d, 1H, J = 7.2 Hz), 7.55 (d, 1H, J = 7.2 Hz), 2.68 (s, 3H), −16.90 (t, 1H, J = 2.0 Hz), −18.02 (t, 1H, J = 2.0 Hz), −18.65 (t, 1H, J = 2.0 Hz).

Thermolysis of 13 in the Presence of H_2. A thermolysis similar to that above of **13** (0.045 g, 0.047 mmol) under hydrogen followed by similar chromatographic separation gave (μ-H)$_3Os_3(CO)_8(\mu_3$-η^2-$CC_8H_5N_2$) (**24**) (0.037 g, 84%) as red crystals after recrystallization from hexane/CH_2Cl_2 at −20 °C. Anal. Calcd for $C_{17}H_8N_2O_8Os_3$: C, 21.75; H, 0.86; N, 2.98. Found: C, 21.98; H, 0.95; N, 3.05. IR (νCO, CH_2Cl_2): 2090m, 2073vs, 2018m, 2012s, 1984s, 1950m cm^{-1}. ^{1}H (NMR, CD_2Cl_2): δ 9.06 (d, 1H, J = 2.4 Hz), 9.76 (d, 1H, J = 2.4 Hz), 7.88 (t, 1H, J = 4.4 Hz), 7.73 (d, 2H, J = 4.4 Hz), 2.66 (s, 3H), −16.93 (t, 1H, J = 2.0 Hz), −18.04 (t, 1H, J = 2.0 Hz), −18.65 (t, 1H, J = 2.0 Hz).

X-ray Structure Analysis of 10 and 12. Suitable crystals of **10** and **12** were coated with Paratone N oil, suspended in a small fiber loop, and placed in a cooled nitrogen gas stream at 173 K on a Bruker D8 SMART APEX CCD sealed tube diffractometer with graphite-monochromated Mo Ka (0.71073 Å) radiation. A hemisphere of data was measured using a series of combinations of phi and omega scans with 10 s frame exposures and 0.3 frame widths. Data collection, indexing, and initial cell refinements were all carried out using SMART[31] software. Frame integration and final cell refinements were done using SAINT[32] software. The final cell parameters were determined from least-squares refinement on 3077 and 4205 reflections, respectively, for **10** and **12**. The SADABS[33] program was used to carry out absorption corrections.

The structures were solved using direct methods and difference Fourier techniques (SHELXTL, V6.12).[34] Hydrogen atoms were placed in their expected chemical position using the HFIX command and were included in the final cycles of least squares with isotropic U_{ij}'s related to the atoms ridden on. The hydrides were positioned by using the XHYDEX program in the WinGX suite of programs.[26] All non-hydrogen atoms were refined anisotropically. Scattering factors and anomalous dispersion corrections are taken from *International Tables for X-ray Crystallography*.[35] Structure solution, refinement, graphics, and generation of publication materials were performed by using SHELXTL, V6.12 software. Additional details of data collection and structure refinement are given in Table 1.

X-ray Structure Analysis of 13, 17, and 20. Crystals of **13**, **17**, and **20** suitable for X-ray diffraction were grown by slow diffusion of hexane into a dichloromethane solution at −4 °C. Crystallographic data were collected at 120 K, using a Bruker-Nonius CCD area detector diffractometer and Mo Kα radiation (λ = 0.71073 Å). Data collection and processing were carried out using the programs COLLECT[36] and DENZO.[37] Empirical absorption corrections were applied to the data set using multiple and symmetry-related data measurements via the program SORTAV.[38,39] The unit cell parameters were indexed from all observed reflections in a θ range of 10° and refined using the entire data set. The structures were solved by direct methods (SHELXS-97)[40] and refined on F^2 by full matrix least-squares (SHELXL-97)[41] using all unique data. The bridging hydrides in **13** were located from a difference map but not refined. All non-hydrogen atoms were refined anisotropically. The hydrogen atoms were included in calculated positions (riding model) with U_{iso} set at 1.2 times the U_{eq} of the parent atom.

Electrochemistry. Electrochemical measurements were performed using a BAS CV-50W analyzer equipped with a standard three-electrode cell. This cell was designed to allow the tip of the reference electrode to approach closely to the working electrode. Voltammetric experiments were performed using aqueous Ag/AgCl as a reference electrode, a glossy carbon as a working electrode, and platimum wire as the auxiliary electrode. Potential data are referred to the ferrocene (0/+) couple, which is oxidized in CH_2Cl_2 at +0.48 V vs Ag/AgCl. Typically, a solution containing 1 mM of the cluster and 0.1 M supporting electrolyte (tetrabutylammonium hexaflurophosphate, Bu_4NPF_6) was prepared using freshly distilled dichloromethane. The solution was degassed prior to introducing the sample and also between runs. Positive feedback *iR* compensation was routinely applied.

Computational Details. DFT calculations were performed using the Gaussian 98 and 03 programs.[42] The molecular structures from single-crystal X-ray structure determinations were used for geometry optimization. We used restricted Becke's three-parameter hybrid functional[43] and Lee−Yang−Parr's gradient-corrected correlation function (B3LYP) through-

(31) *SMART* Version 5.628; Bruker AXS, Inc.: Madison, WI, 2003.
(32) *SAINT* Version 6.36; Bruker AXS, Inc.: Madison, WI, 2002.
(33) Sheldrick, G. *SADABS* Version 2.10; University of Göttingen, 2003.
(34) SHELXTL V6.12; Bruker AXS, Inc.: Madison, WI, 2003.
(35) Wilson, A. J. C., Ed. *International Tables for X-ray Crystallography, Volume C*; Kynoch, Academic Publishers: Dordrecht, 1992; Tables 6.1.1.4 (pp 500−502) and 4.2.6.8 (pp 219−222).
(36) Hooft, R. *COLLECT Data Collection Software*; Nonius B.V., Delft: The Netherlands, 1998.
(37) Otwinowski, Z.; Minor, W. In *Macromolecular Crystallography*; Carter, C. W., Jr., Sweet, R. M., Eds.; Academic Press: New York, 1997; pp 307−326.
(38) Blessing, R. H. *Acta Crystallogr.* **1995**, *A51*, 33.
(39) Blessing, R. H. *J. Appl. Crystallogr.* **1997**, *30*, 421.
(40) Sheldrick, G. M. *Acta Crystallogr. Sect. A* **1990**, *46*, 467.
(41) Sheldrick, G. M. *SHELXL-97*, *Program for Crystal Structure Refinement*; University Göttingen: Germany, 1997.
(42) Closson, W. D.; Wriede, P.; Bank, S. *J. Am. Chem. Soc.* **1966**, *88*, 1581.

out.[44] The basis sets employed were LanL2dz for the osmium atoms, using the relativistic effective core potential (ECP), which replaces the inner core electrons, and 6-31G for the other atoms in all the calculations. No symmetry restrictions were placed on the optimizations. Stationary points were determined by performing normal-mode analyses on the optimized structures.

(43) Becke, A. D. *J. Chem. Phys.* **1993**, *98*, 5648.
(44) Lee, C.; Yang, W.; Parr, R. G. *Condens. Matter* **1988**, *37*, 785.

Acknowledgment. We gratefully acknowledge the Royal Society of Chemistry for a research grant. E.R. thanks the Department of Energy for support.

Supporting Information Available: Text and tables giving details of the X-ray crystallographic structure determination for **10**, **12**, **13**, **17**, and **20**. This material is available free of charge via the Internet at http://pubs.acs.org.

OM0503794